Journal of Materials Science and Chemical Engineering, 2025, 13(10), 19-37
https://www.scirp.org/journal/msce
ISSN Online: 2327-6053
ISSN Print: 2327-6045

Performance Enhancement of Lead-Free K_2TiI_6-Based Perovskite Solar Cells Using SCAPS-1D Simulation Study

Rony Tota*, Tarikul Islam Tasin, Shak Mahmudul Hasan, Md. Morsalin, Zamil Sultan, Muien Ahmed Arnob, Mehedi Hasan Tanim, Najiba Abedin Sajan

Department of Electrical and Electronic Engineering, Hajee Mohammad Danesh Science and Technology University, Dinajpur, Bangladesh
Email: *ronytota98@gmail.com

How to cite this paper: Tota, R., Tasin, T.I., Hasan, S.M., Morsalin, M., Sultan, Z., Arnob, M.A., Tanim, M.H. and Sajan, N.A. (2025) Performance Enhancement of Lead-Free K_2TiI_6-Based Perovskite Solar Cells Using SCAPS-1D Simulation Study. *Journal of Materials Science and Chemical Engineering*, **13**, 19-37.
https://doi.org/10.4236/msce.2025.1310002

Received: September 20, 2025
Accepted: October 25, 2025
Published: October 28, 2025

Abstract

Perovskite solar cells (PSCs) have emerged as one of the most promising candidates for future renewable energy solutions due to their low cost, ease of fabrication, and potential for high efficiency. The lead-free perovskite element in this study demonstrates a high absorption coefficient and an optimal optical band, making it a suitable candidate for sustainable photovoltaic technologies. The goal of the experiment was to optimise the device's defect density, acceptor density (N_A), donor density (N_D), and absorber thickness. Fluorine-doped tin-oxide (FTO) was used as the window layer, D-PBTTT-14 as the hole transport layer (HTL), Au as the back layer, K_2TiI_6 as the absorber layer, and CdZnS as the electron transport layer (ETL) to improve device performance. This study employs a PSC based on K_2TiI_6 and SCAPS-1D simulation to evaluate its structural, photovoltaic, and optical properties. In particular, the effects of carrier concentration, absorber thickness, and defect densities were thoroughly studied and analysed via simulation. Significant improvements in open-circuit voltage (Voc), FF, and efficiency were observed with the implementation of this solar cell (SC). The study also investigates the impact of operating temperature on efficiency and other electrical properties. Optimisation of the material thicknesses was performed to achieve the desired target. The optimised cell structure, FTO/CdZnS/K_2TiI_6/D-PBTTT-14/Au, achieved a FF of 86.50%, an Voc of 1.33 V, a short circuit current density (Jsc) of 24.42 mA/cm^2, and a high performance efficiency of 28.11%. Factors such as operating temperature, electron affinity, surface recombination velocity, series resistance, shunt resistance, and buffer/absorber and absorber/HTL interference were carefully optimised to enhance performance. In conclusion, lead-free PSCs

based on K_2TiI_6 present a highly promising option for sustainable energy solutions, contributing to the development of cost-effective and high-efficiency photovoltaic technologies.

Keywords

Lead-Free PSCs, K_2TiI_6, SCAPS-1D Simulation, ETL, HTL, Power Conversion Efficiency (PCE), Device Optimisation, Interface Defects, Quantum Efficiency (QE)

1. Introduction

Traditional energy sources like gas, oil, and coal are heavily relied upon to meet significant energy demands, despite their negative environmental impacts and contribution to climate change. However, the supply of these resources is also finite. Consequently, experts are continuously exploring ways to transition from these conventional energy sources to renewable alternatives, such as hydropower, solar, and wind energy. Solar energy, in particular, plays a key role in producing eco-friendly power due to its abundance; the energy provided by sunlight globally exceeds that of all other renewable sources combined [1]. Solar energy production is more than capable of meeting the energy needs of humanity, even in the most technologically advanced societies. However, solar energy must be harvested, processed, and stored to address the challenges posed by its daily cycles and intermittent nature. PV cells, which convert light into electricity, serve as the primary components for capturing this. A third-generation PV cell, called perovskite, offers potential to rival traditional solar technologies due to its easier manufacturing process and lower production costs [2]. One common design used in SCs is a one-dimensional n-i-p flat heterojunction, which is composed of multiple semiconductor layers. PSCs have gained significant attention in recent years because of their potential for high-efficiency and cost-effective solar energy conversion [3], [4]. While lead-based PSCs demonstrate excellent efficiency, concerns about lead toxicity have led researchers to investigate lead-free alternatives [5]-[7]. One promising candidate is the $CsSnCl_3$ perovskite absorber layer, which has shown potential for achieving high efficiency without using lead [8]. Among the various materials being studied for PSCs, Potassium Titanium Hexahelied (K_2TiI_6), a lead-free alternative, is particularly noteworthy. Kumar *et al.* (2022) first synthesized K_2TiI_6 perovskite material for photovoltaic applications, highlighting its promising optical properties, direct bandgap of 1.61 eV, and remarkable stability, making it suitable for single-junction solar cell fabrication [9]. They conducted a performance investigation of K_2TiI_6-based perovskite solar cells, achieving a maximum efficiency of 4.38% with the configuration FTO/ZnO/K_2TiI_6/PEDOT: PSS [9]. Further investigations were carried out by Singh *et al.* (2024), who initially achieved an efficiency of 5.70% with the configuration FTO/TiO_2/K_2TiI_6/PEDOT: PSS. After optimization, they improved the efficiency to 23.75% with the config-

uration FTO/PCBM/K_2TiI_6/$Sr_2Cu_2O_2$ [10]. PSCs have emerged as a promising technology for efficient and affordable energy conversion. In this study, we combine CdZnS as the ETL and D-PBTTT-14 as the HTL to enhance performance. CdZnS is a crucial ETL material for K_2TiI_6-based SC applications, as it can be tuned to optimize the band alignment at the ETL/K_2TiI_6 interface, reducing non-radiative recombination and enhancing the efficiency of the SCs [11]. The Shockley-Queisser (SQ) limit for SC defines the maximum theoretical efficiency for a single-junction solar cell, which is typically 33.7% for an ideal 1.4 eV band-gap material. This efficiency limit accounts for energy losses that occur through various mechanisms such as thermalization, in-band loss, and entropy generation. For materials with a 1.61 eV band gap, such as K_2TiI_6, the theoretical maximum efficiency would be slightly different, potentially reaching up to 31% - 32% [12] [13]. The efficiency of such SCs largely depends on the bulk defect density of the absorber layer, which can be modified to optimise performance. To further investigate the impact of changes in bulk defect density, researchers use simulation tools like SCAPS to analyse SC behaviour under different conditions [14]. These simulations aim to improve the efficiency and stability of PSCs for wider renewable energy applications. By varying the defect density (N_t) of the active layer, the performance of the K_2TiI_6-based PSC can be effectively evaluated. The results reveal that PV parameters are significantly optimized when the defect density is minimized. At the lowest defect density (10^{11} cm^{-3}), we obtained the FF is 86.50%, the Jsc is 24.42 mA/cm^2, the Voc is 1.33 V, and the power conversion efficiency (PCE) is 28.11% which is superior to previous studies [9] [10]. The study utilized the SCAPS simulation tool, which can model devices with multiple semiconductor layers, to perform numerical simulations.

2. Methodology

Figure 1 shows the planned PSC structure (FTO/CdZnS/K_2TiI_6/D-PBTTT-14/Au) with K_2TiI_6 as the absorber layer, which has a substantial influence on PV parameters due to its optical absorption properties and **Figure 2** shows the crystal structure of K_2TiI_6. **Figure 3** illustrates the schematic energy band diagram of the proposed PSC structure. The PSC architecture uses D-PBTTT-14 and Fluorine doped-Tin-Oxide (FTO) as HTL and TCO, respectively, with Glass and Au acting as front and back contacts. The interplay between ETL and HTL impacts the transport and extraction of charges in the absorber layer, altering critical parameters such as Voc, PCE, FF, and Jsc. The Voc is affected by the difference in Fermi energy levels between the ETL and HTL. The SC receives illumination of 100 mW/cm^2 from the AM 1.5 G solar spectrum at 300 K working temperature. We analyzed optimal settings for series (Rs) and shunt (Rsh) resistances in the SC construction. The proposed structure and performance parameters were simulated using "The one-dimensional simulation program, SCAPS-1D", for the SC Capacitance Simulation, which was created by Burgelman and colleagues at the University of Gent, Belgium's Department of Electronics and Information Systems [15]. Researchers studying SCs can effectively analyze device structures using SCAPS-1D.

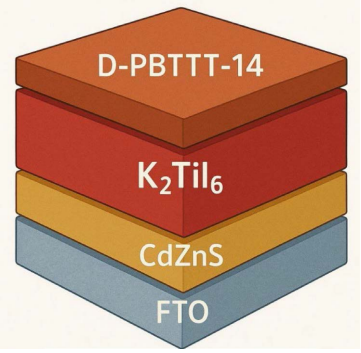

Figure 1. Design configuration of the K_2TiI_6-based PSC.

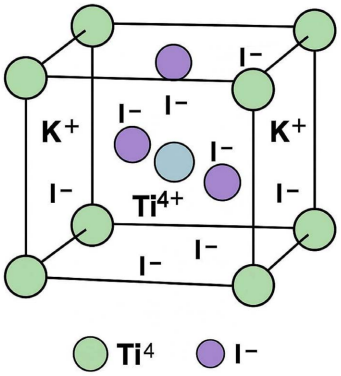

Figure 2. The optimized crystal structure of K_2TiI_6 perovskite.

This instrument performs a fantastic job of examining the spectrum and electrical responses of SCs. Table 1 and Table 2 present the input parameters used for thin-film SC simulations, as compiled from previous research studies.

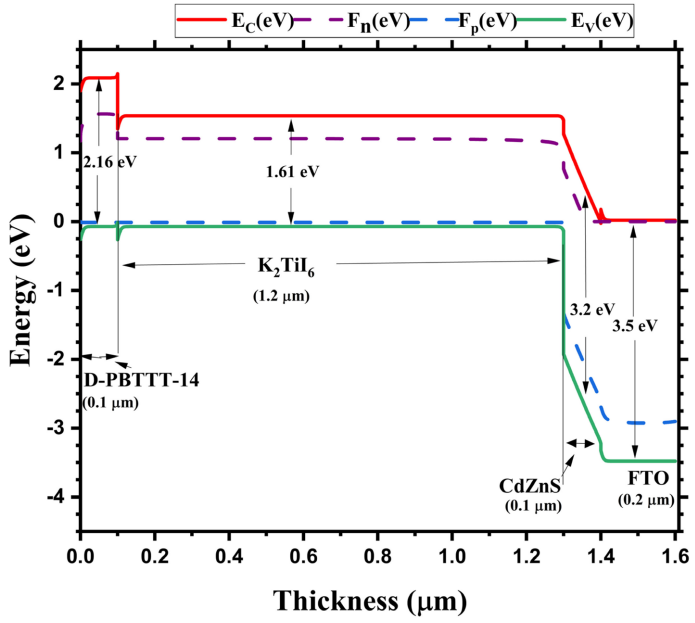

Figure 3. Schematic energy band diagram of the proposed PSC structure.

Table 1. Input optimization parameters of TCO, ETL, and absorber layer of the study [9] [16].

Parameters	FTO	CdZnS	K_2TiI_6	D-PBTTT-14
Thickness (nm)	200	100	1200	100
E_g (eV)	3.5	3.2	1.61	2.16
χ (eV)	4	4.2	4	3.2
ε_r (relative)	9	9.12	4.2	10
N_c (cm^{-3})	2.2×10^{18}	1.5×10^{18}	1×10^{19}	2.8×10^{19}
N_v (cm^{-3})	1.8×10^{19}	1.8×10^{18}	1×10^{19}	1×10^{19}
μ_n ($cm^2 \cdot V^{-1} \cdot s^{-1}$)	20	250	4.4	2.83×10^{-3}
μ_p ($cm^2 \cdot V^{-1} \cdot s^{-1}$)	10	40	2.5	2.83×10^{-3}
N_A (cm^{-3})	1×10^{18}	1×10^{16}	0	0
N_D (cm^{-3})	0	0	1×10^{18}	1×10^{18}
N_t (cm^{-3})	$1 \times 10^{15*}$	$1\times 10^{14*}$	$1 \times 10^{13*}$	$1 \times 10^{14*}$

Here, $\mathbf{E_g}$: Bandgap, $\boldsymbol{\chi}$: Electron Affinity, $\boldsymbol{\varepsilon_r}$: Dielectric permittivity, $\mathbf{N_c}$: CB effective DOS, $\mathbf{N_v}$: VB effective DOS, $\boldsymbol{\mu_n}$: Electron mobility, $\boldsymbol{\mu_p}$: Hole mobility, $\mathbf{N_A}$: Shallow uniform acceptor density, $\mathbf{N_D}$: Shallow uniform donor density and $\mathbf{N_t}$: Defect density.

Table 2. Interface defect densities between different layers [9] [16].

Interface	Defect type	Capture cross section: Electrons/holes (cm^2)	Energetic Distribution	Reference for defect energy level	Total density (cm^{-3}) (integrated overall energies)
ETL/K_2TiI_6	Neutral	1.0×10^{-17} 1.0×10^{-18}	Single	Above the VB maximum	1.0×10^{10}
K_2TiI_6 /HTL	Neutral	1.0×10^{-18} 1.0×10^{-19}	Single	Above the VB maximum	1.0×10^{10}

3. Results and Discussions

3.1. Absorber Layer Defect Density Variation Effect

Figure 4 shows the absorber defect density (Nt) variation (range from 10^{13} to 10^{18} cm^{-3}) effect on PV performance. Researchers have explored K_2TiI_6 as a potential absorber layer for perovskite-inspired PV SCs due to its promising optoelectronic properties. and FTO/ETL/K_2TiI_6/HTL/Au the PV cell, which had CdZnS as an ETL layer, had the best efficiency at 28.11%, which means that charge carriers were moved and extracted efficiently. It had a Jsc of about 24.42 mA/cm^2, which means it either absorbed light better or generated and moved charge carriers more efficiently.

The Voc was about 1.33 V, which shows that ETL helps keep the potential difference between the electrodes high and stops charges from recombining and FF of about 86.5%, which means that there were few resistance losses, good charge extraction, and good carrier collection. The lower current says that there

are some limits on how charges can be created or moved. The Voc decreases after increase defect density from 1E13 to 1E18. These findings are clearly illustrated in Figure 4.

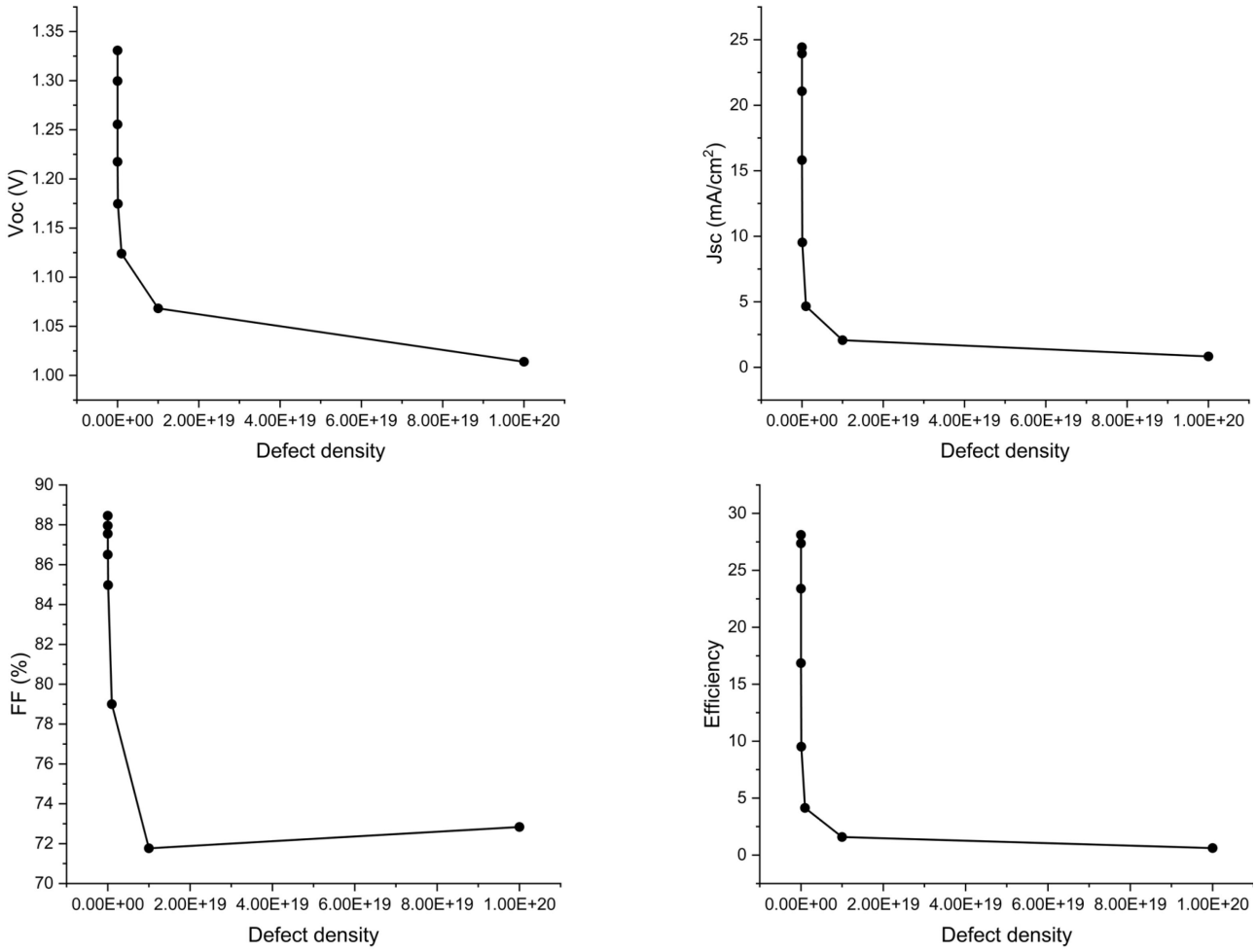

Figure 4. The variation of absorber layer (K_2TiI_6) defect density.

3.2. Absorber Layer Doping Density Variation

Figure 5 presents an analysis of how absorber doping concentration (from 10^{13} to 10^{20} cm^{-3}) influences PV cell performance by examining key parameters such as FF, Voc, Jsc, and overall efficiency. The findings demonstrated that increasing doping concentration typically increased Jsc. At a doping level of 10^{18} cm^{-3}, the CdZnS cell achieved the highest value of 24.42 mA/cm^2. At the greatest doping concentration, ETL showed lower Jsc values, increasing from 4.66 mA/cm^2 to 24.4 mA/cm^2. Voc values, on the other hand, varied considerably. Up to a doping concentration of 1×10^{13} cm^{-3}, showed constant Voc; beyond that, a fall took place; CdZnS peaked at 24.48 mA/cm^2 and dropped to 4.66 mA/cm^2.

When doping was increased, FF values improved marginally, especially above 1×10^{14} cm^{-3}. At the greatest doping concentration. The FF trends were similar to

those of 85.84%. The results emphasize how crucial it is to maximize doping concentration to counteract potential drops in Voc and balance enhanced Jsc and FF, thereby improving solar efficiency.

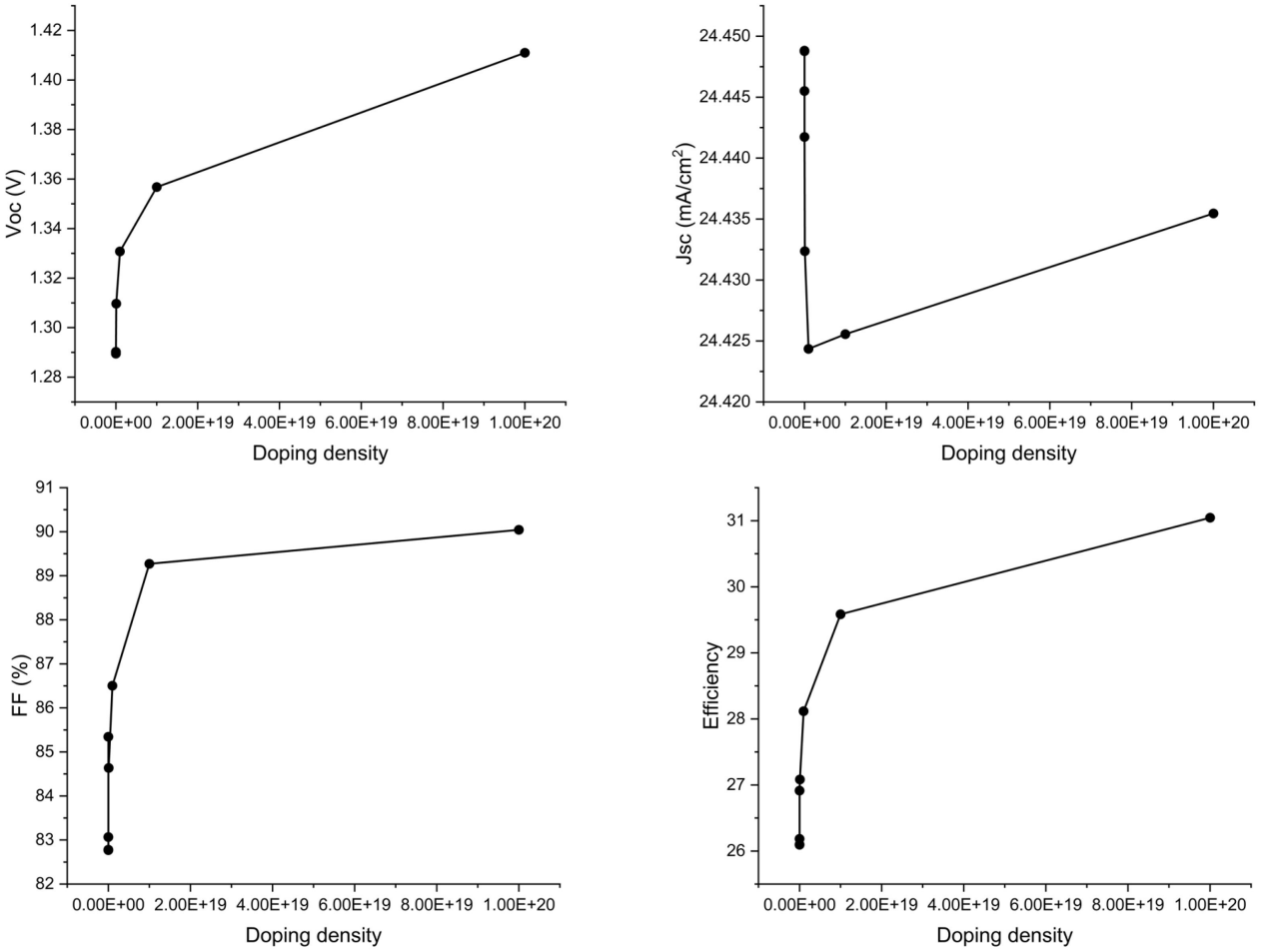

Figure 5. The variation of absorber layer (K_2TiI_6) doping density.

3.3. Absorber Layer Thickness Variation

In SCs, the efficiency usually rises with absorber layer thickness because of improved photon absorption. However, because of recombination losses, a little decrease in efficiency is seen beyond 1.2 μm thickness. **Figure 6** illustrates that absorber layer demonstrates the highest efficiency among the materials studied, reaching a peak of overall 28% at 1.2 μm. Though the higher thickness of 1.2 μm shows high efficiency but it does not increase too much. Better charge carrier separation and enhanced light absorption are associated with higher Jsc. On the other hand, when thickness grows, the Voc significantly lowers. This implies that resistive losses or other variables lower FF while Jsc and Voc improve.

The FF is 86.5%, and Jsc is 24.48 mA/cm^2. And the higher thickness also experiences comparable drops. The reduction in efficiency is attributed to a small decrease in FF and decreasing enhancements in Jsc for thicknesses over 1.2 μm, not-

withstanding increased Voc and Jsc.

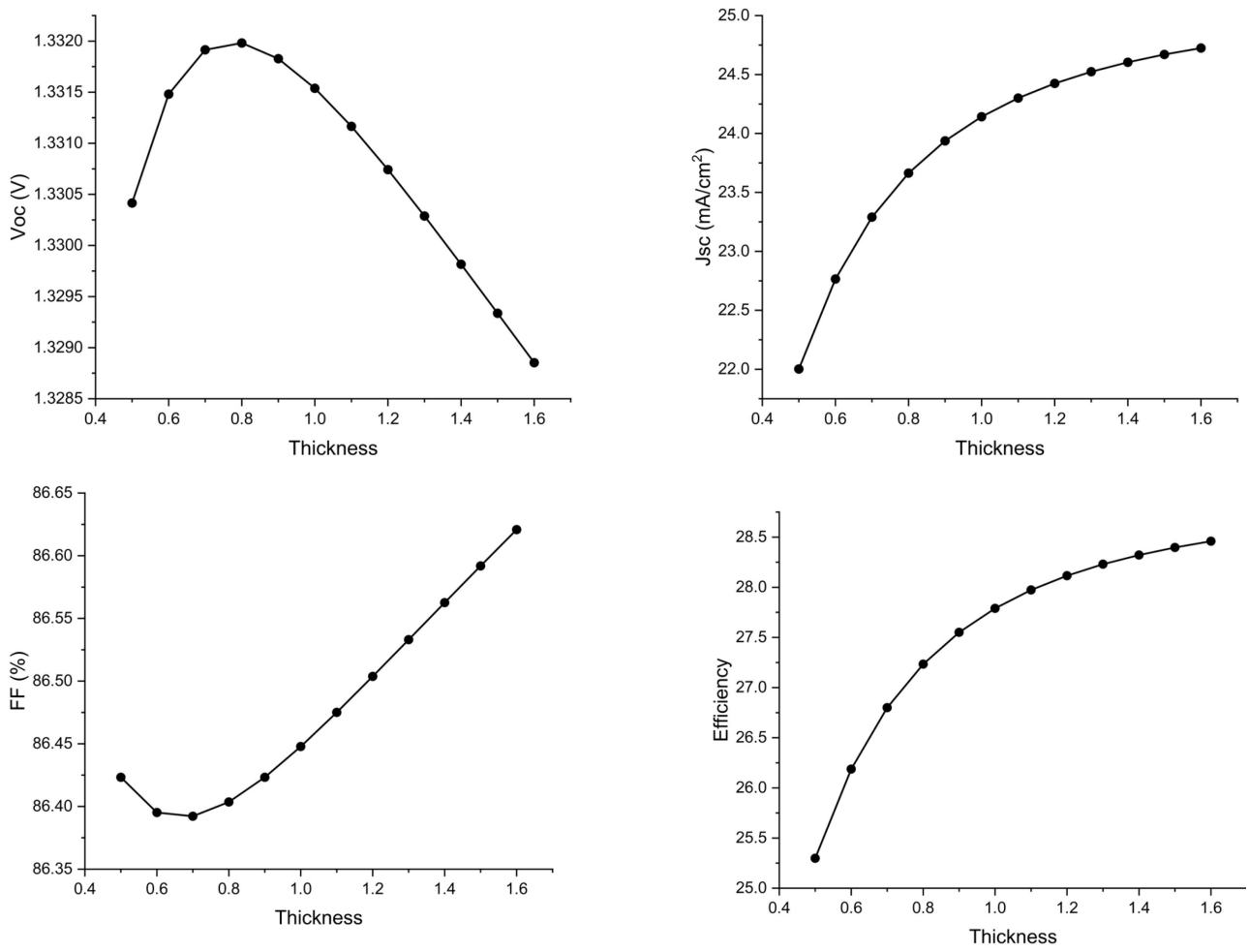

Figure 6. The variation of absorber layer (K_2TiI_6) thickness.

3.4. ETL (CdZnS) Defect Density Variation

Figure 7 reveals that CdZnS maintained remarkably stable efficiency values of 28.11% and 28.07%, respectively, across a range of defect densities. Conversely, at increasing defect densities demonstrated a considerable decrease in efficiency, starting at 28.11% and decreasing to 27.82%. Given that increasing defect density creates recombination centers, which reduce charge collection, this implies that ETL are more resistant to changes in defect density. whereas ETL layer is more susceptible. As defect density grew, the Jsc values decreased from 24.42 mA/cm^2 to 24.25 mA/cm^2 respectively. This shows that the potential difference goes down as the number of defects goes up because of recombination less losses in CdZnS.

All of the materials kept their Voc at 1.33 V, which shows that flaw density doesn't have a big effect on internal resistance and charge transport. Efficiency trends behind Jsc and Voc. Across all defect densities, CdZnS exhibited consistent FF levels of 86.50% and 86.24%, respectively. The FF indicates that it is less sensi-

tive to fault density. While FF was constant, also both Jsc and Voc. In conclusion, CdZnS exhibits good stability across defect densities.

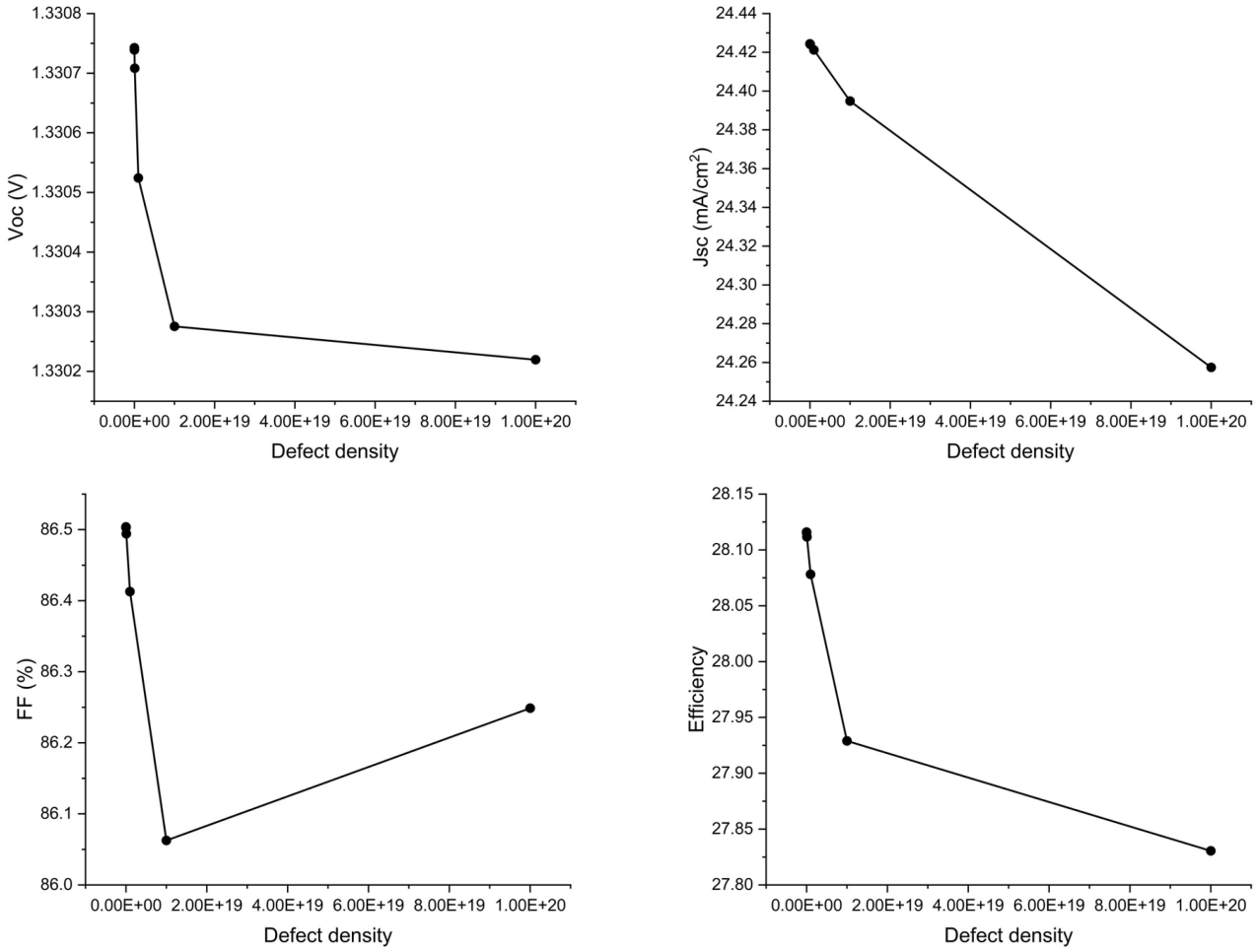

Figure 7. The variation of ETLs (n) defect density.

3.5. ETL (CdZnS) Doping Density Variation

With increasing doping concentrations, the efficiency values for CdZns gradually increase. As shown in **Figure 8**, the efficiency of CdZns increases from 28.16% to 27.74%. This enhancement is likely due to improved charge carrier collection and reduced recombination rates. On the other hand, efficiency appears to have a slightly constant value. For CdZnS, Jsc is constant at around 26.24 - 26.25 mA/cm^2 and is not impacted by doping concentrations.

Nevertheless, Jsc decreases from 24.42 mA/cm^2 to 24.43 mA/cm^2, suggesting that increased doping adds recombination sites, which lowers the potential difference. For CdZnS, the Voc stays constant at 1.33 eV to 1.38 eV range indicating improved charge collection at higher doping levels. Doping increases the FF materials. CdZnS climbs from 86.66% to 89.55%. While Voc goes down. In conclusion, increasing doping steadily increases Jsc and efficiency for ETL layer. Higher doping levels improve the performance of all three materials showing the most

efficiency improvement.

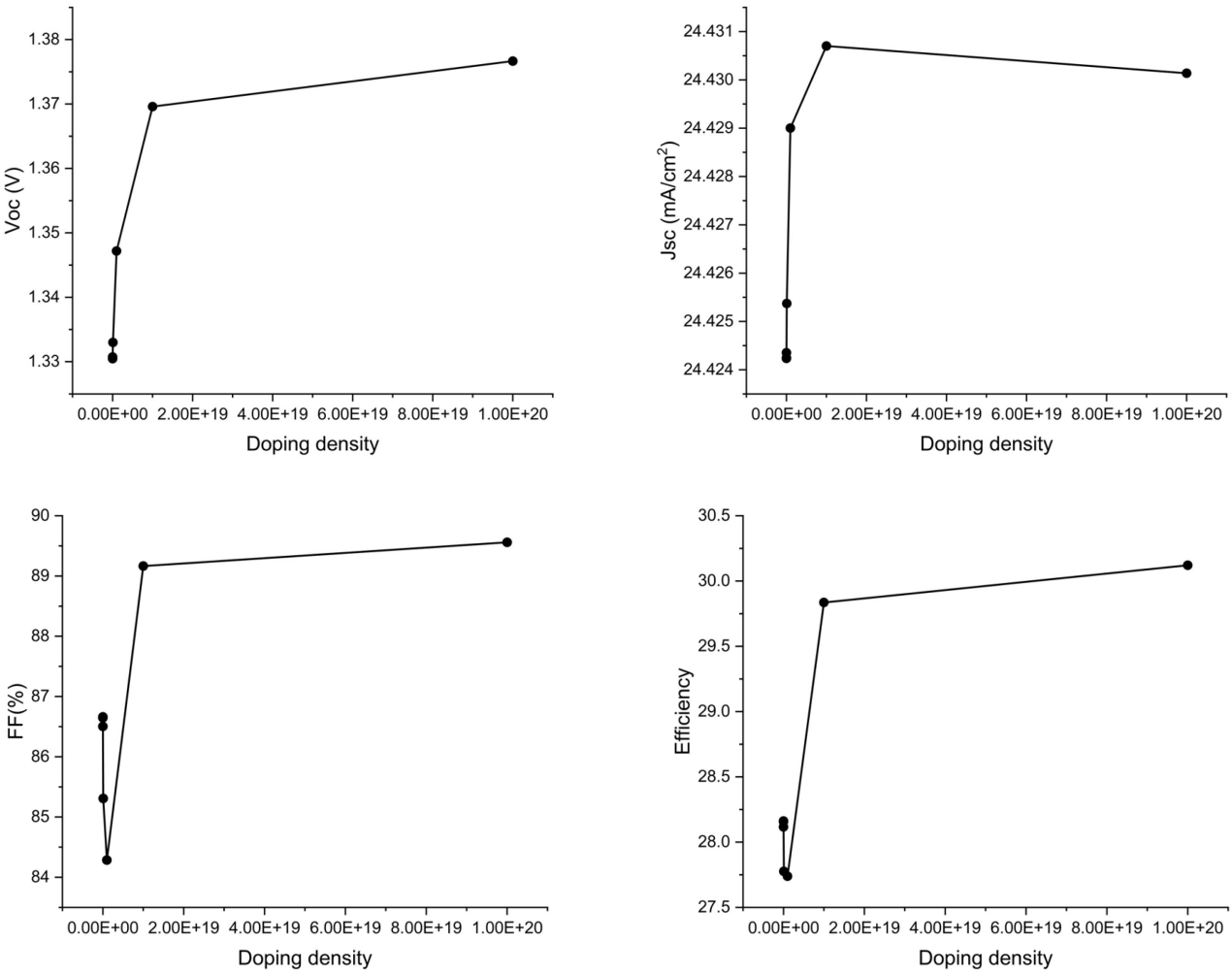

Figure 8. The variation of ETLs doping density.

3.6. ETL (CdZnS) Thickness Variation

Figure 9 shows that variations in ETL thickness lead to increased efficiency values and reveal distinct performance patterns for each material. The efficiency of CdZnS shows a little bit increase, going from 28.05% at 0.06 μm to 28.13% at 0.15 μm. With just little variation is still comparatively steady.

This is probably because, as the ETL thickens, resistive losses rise and carrier flow decreases. ZnSe also exhibits little fluctuation, falling from 24.425 mA/cm^2 to 24.423 mA/cm^2, whereas Jsc for look like stays constant. Conversely, as ETL thickness grows, Jscnet affects much. It is most likely as a result of recombination fewer losses. The Voc stays at 1.3309 V at 0.06 μm to 1.3306 eV at 0.15 μm, demonstrating steady charge transport characteristics. FF trends are similar to Voc and Jsc trends. They stay steady, exhibiting only minor changes between 86.28% and 86.56%, at increasing ETL thicknesses. In conclusion, ETL thickness grows, CdZnS remains stable throughout a range of ETL thicknesses.

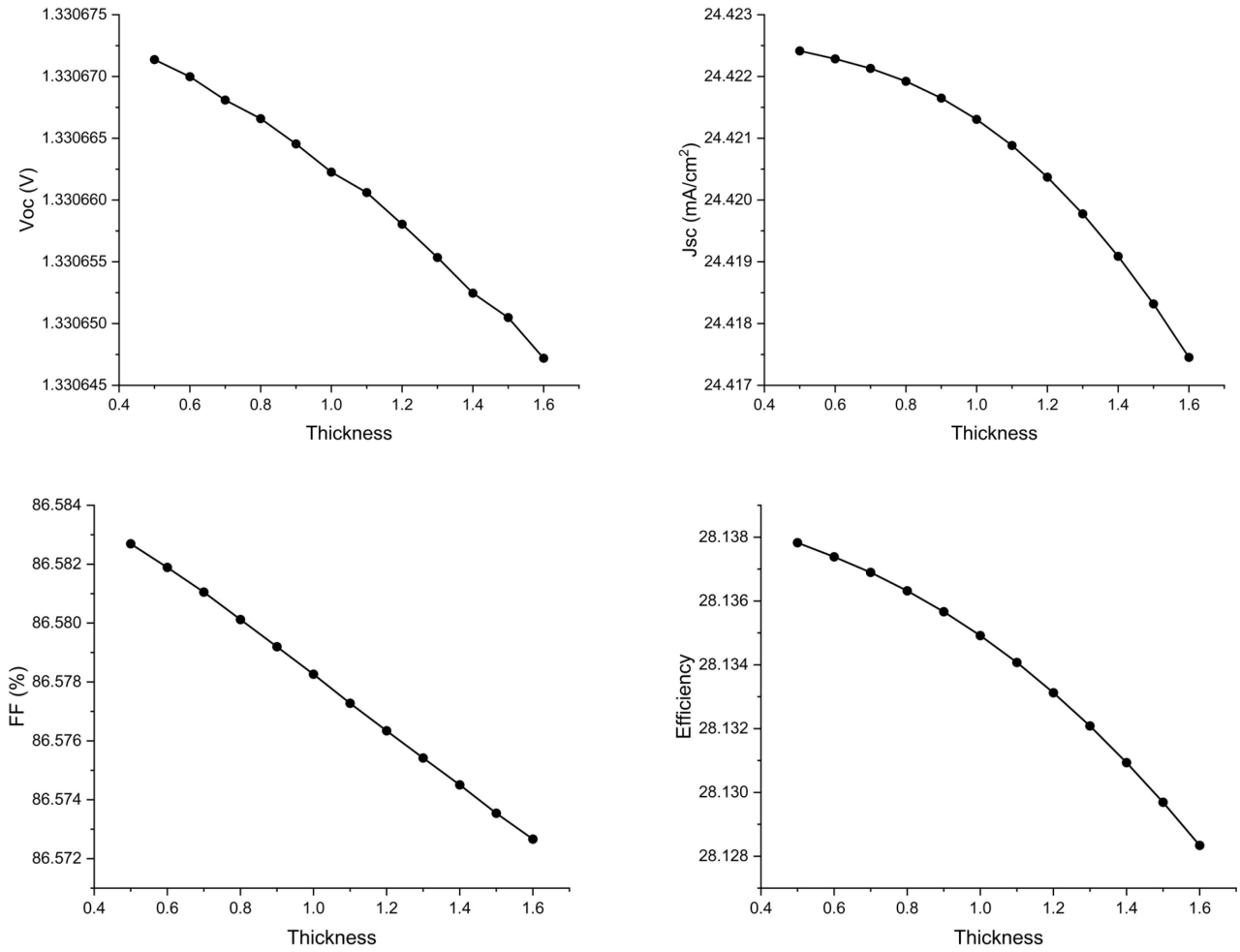

Figure 9. The variation of ETLs thickness.

3.7. HTLs (D-PBTTT-14) Defect Density Variation

Figure 10 demonstrates that for HTL layer, the efficiency, Voc, FF, and Jsc remain unchanged across the entire range of HTL defect densities. This indicates a high resistance of these materials to HTL defect states, which consistently maintains values of 28.11% efficiency, 24.42 mA/cm^2 Jsc, 1.33 V Voc, and 86.50% FF. Similarly shows stable performance efficiency.

All materials exhibit the same efficiency, indicating that they are not significantly affected by recombination losses when it comes to charge carrier collection and that they are thus resistant to changes in HTL defect density. Similarly, continuous Voc indicates maintained internal resistance and charge transport capabilities, and steady Jsc values show that HTL defect density does not affect charge separation or the built-in potential.

The efficiency levels stay the same, which suggests that the HTL defect density doesn't have a big effect on the performance of SCs. This means that the HTL defect density doesn't have a big effect on the PV performance of these materials.

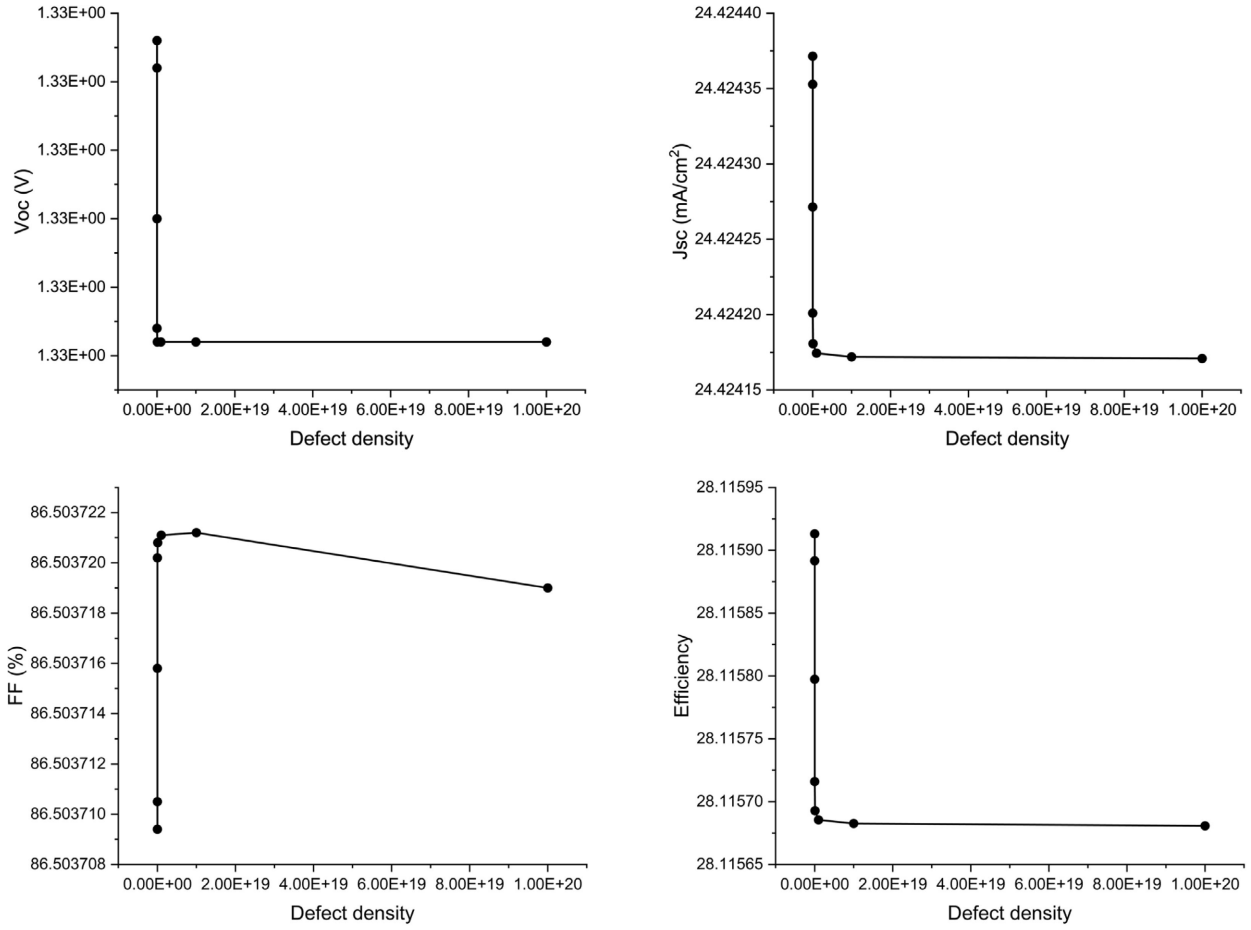

Figure 10. The variation of HTLs (D-PBTTT-14) defect density.

3.8. HTLs (D-PBTTT-14) Doping Density Variation

The efficiency values grow gradually with increasing HTL doping concentration, indicating enhanced charge carrier transit and decreased recombination losses. Rising from 21.53% to 22.12%, WS_2 has the biggest rise, from 26.3% to 28.3%.

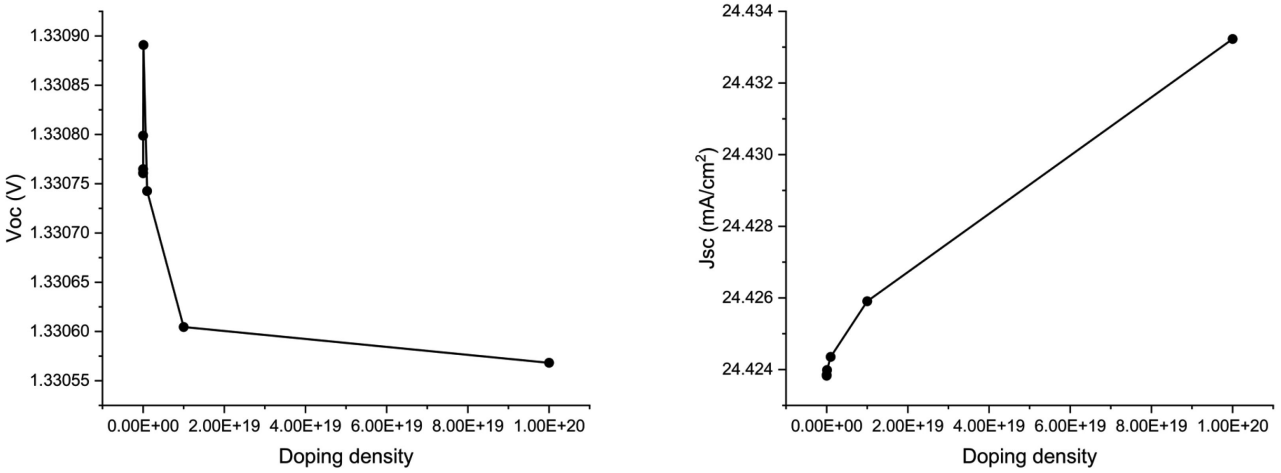

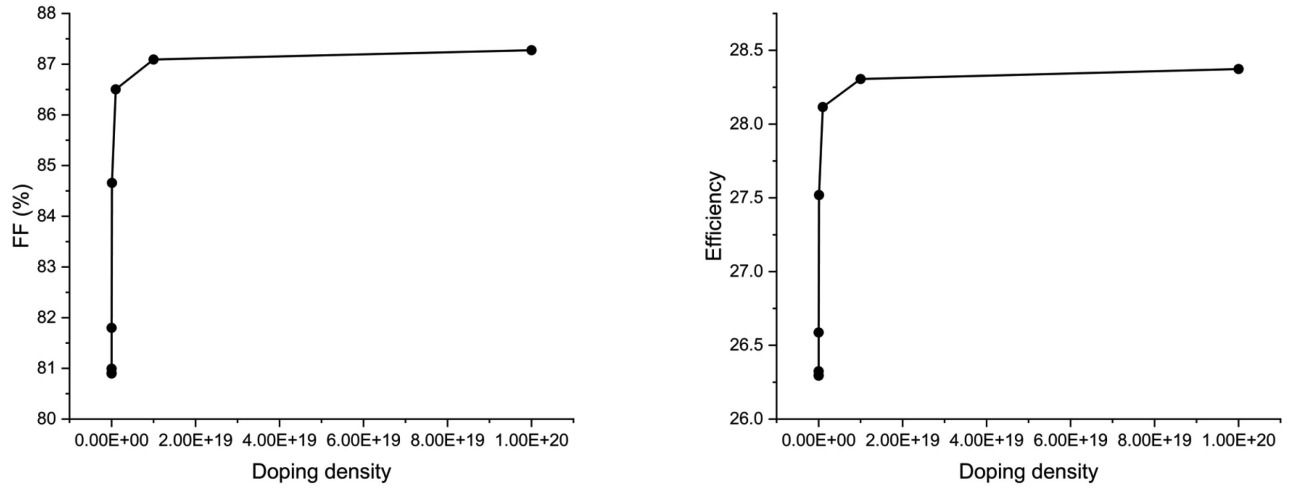

Figure 11. The variation of HTLs (CBTS) doping density.

This suggests improved carrier collection from photogenerated light. Doping concentration also slightly improves Jsc values rise to 24.42 mA/cm^2 to 24.43 mA/cm^2. Higher doping appears to improve charge separation and the intrinsic potential, based on this stability. For all three materials, the Voc stays constant at 1.33 eV, suggesting that increasing doping does not result in resistive losses or impair charge transfer. **Figure 11** illustrates that efficiency improves with increasing doping concentration. It shows the most significant gain, rising from 80.9% to 87.12% which follows with an increase 7.03%.

Higher efficiency values and marginally improved Jsc values indicate improved overall performance since doping concentration increases carrier mobility and lowers recombination losses, which in turn accounts for the efficiency with the most performance gain.

3.9. Impact on PV Parameters for the Variation of HTLs (D-PBTTT-14) Thickness

As the HTL thickness increases, the efficiency values for D-PBTTT-14 remain largely stable with minimal variation decreases slightly from 28.11% to 28.01%, improving marginally as shown in **Figure 12**.

This stability suggests that HTL thickness does not affect the current generation, which is probably because the materials have effective charge transfer capabilities. For all three materials, the Jsc values marginally rise with thicker HTLs. Enhancements are seen as stable. This implies that charge carrier separation and the built-in potential are somewhat enhanced by a thicker HTL. For all materials, Voc is constant at 1.33 eV even at different HTL thicknesses. This consistency implies that internal resistance and charge transfer are unaffected by HTL thickness, resulting in consistent device performance.

Additionally, overall FF has not altered. 86.3% to 86.1%. This consistency may be explained by the consistent Jsc, Voc, and FF values, which show that HTL thickness within the studied range does not affect the SCs' overall PV performance.

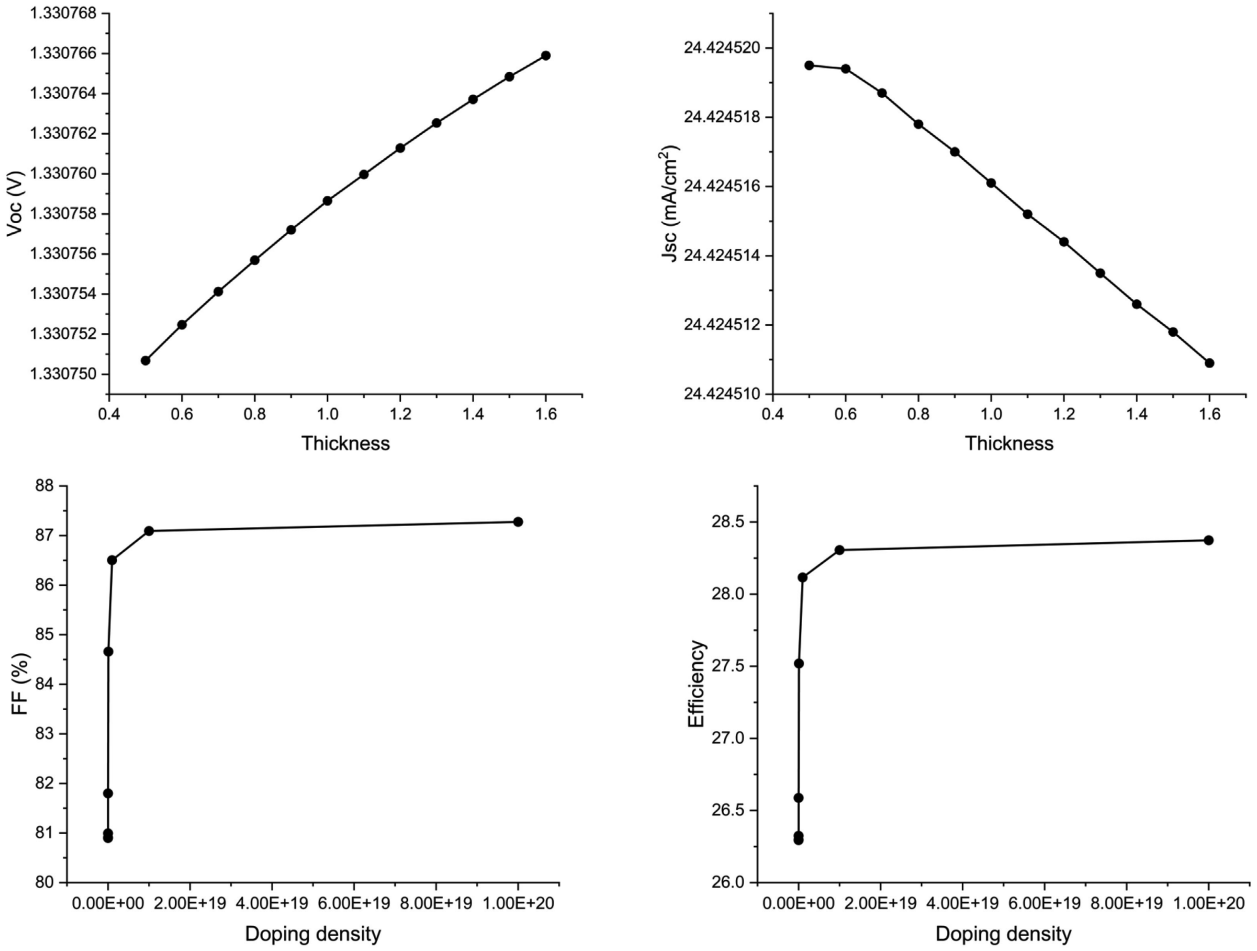

Figure 12. The variation of HTLs (D-PBTTT-14) thickness.

3.10. The Capacitance and Mott-Schottky Lines

The effects of capacitance and Mott-Schottky (M-S) behavior under voltage variation from −0.8 V to +0.8 V for four different configurations are illustrated in **Figure 13**, **Figure 14**. The analysis was conducted at a high frequency of 1 MHz to suppress the influence of deep-level trap states. As shown in **Figure 13**, capacitance increases exponentially with rising forward bias, indicating charge accumulation in the depletion region. The curves are nonlinear and exhibit multiple intersections, reflecting the complex nature of the device interfaces. This configuration, the CdZnS-based ETL structure exhibits the highest capacitance at 0.8 V.

This behavior suggests that under zero or reverse bias, the device operates within the depletion region. As the depletion width approaches the thickness of the absorber layer under forward bias, a rapid increase in capacitance is observed. Conversely, under reverse bias, the capacitance significantly decreases due to increased saturation current and widening depletion width.

The Mott-Schottky (M-S) plots, as shown in **Figure 14**, reveal diffusion potentials and provide insight into defect density. The slope of the $1/C^2$ vs. V curve reflects the defect concentration in the device. A steeper slope indicates lower de-

fect density, while a shallower slope implies higher trap states. Across all structures studied, the M-S values decreased with increasing voltage, aligning with previously reported studies and confirming the presence of interface states and carrier dynamics influenced by applied bias.

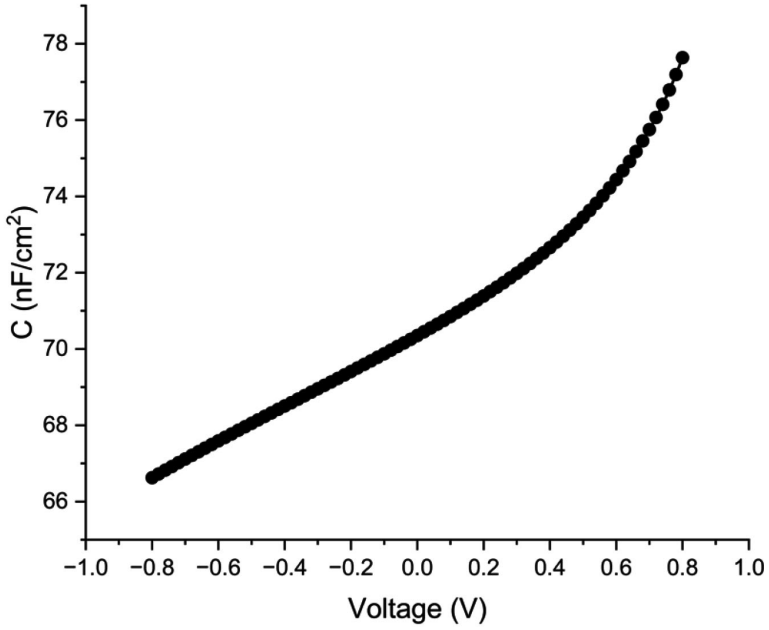

Figure 13. Capacitance-Voltage characteristics of CdZnS-Based devices

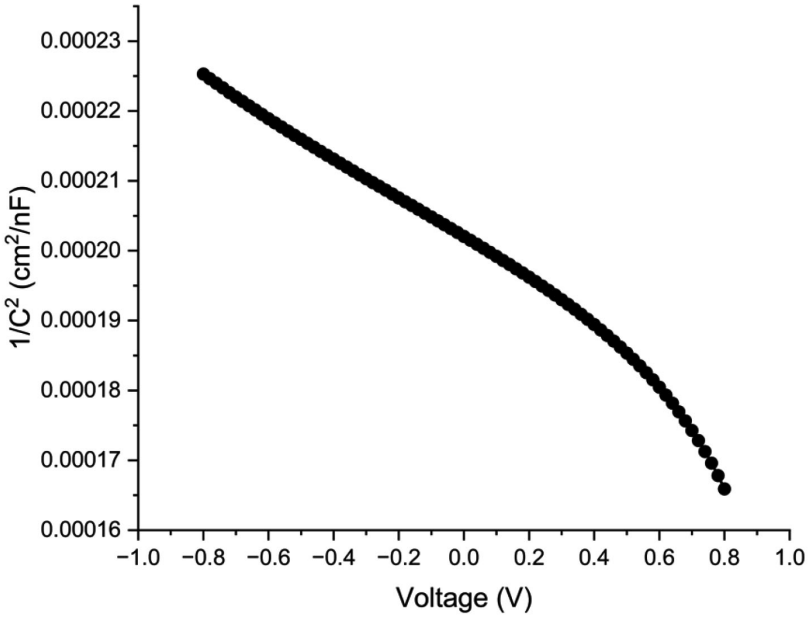

Figure 14. Mott-Schottky behavior with voltage.

3.11. The Generation and Recombination Rate

The charge carrier generation and recombination characteristics of CdZnS reveal

distinct behaviors across varying bias voltages, offering critical insights into their photoelectric performance. As shown in Figure 15, demonstrates an oscillatory generation rate—starting at 7.5 units at 0 V, dipping to 2.72 at 0.2 V, peaking again at 5.88 at 0.4 V, and declining to 2.03 at 1 V.

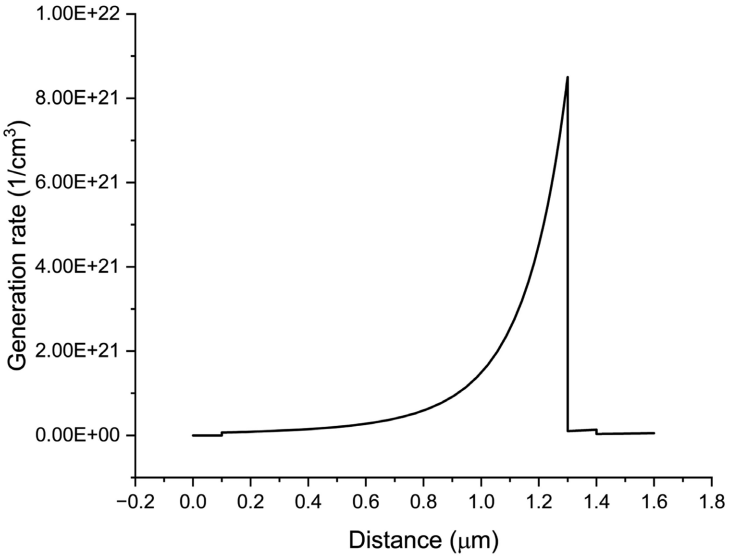

Figure 15. Generation rate profile across the thickness of K_2TiI_6-Based devices.

Recombination behaviors, depicted in Figure 16, show that CdZnS initially has high recombination rates at 0 V—2.59×10^{15} and 2.53×10^{15} units, respectively—which decrease as the bias increases. While starting with the highest recombination rate at 0 V (2.94×10^{15} units), exhibits more consistent and stable recombination levels under higher voltages. This indicates improved carrier extraction efficiency and reduced recombination losses under operating conditions.

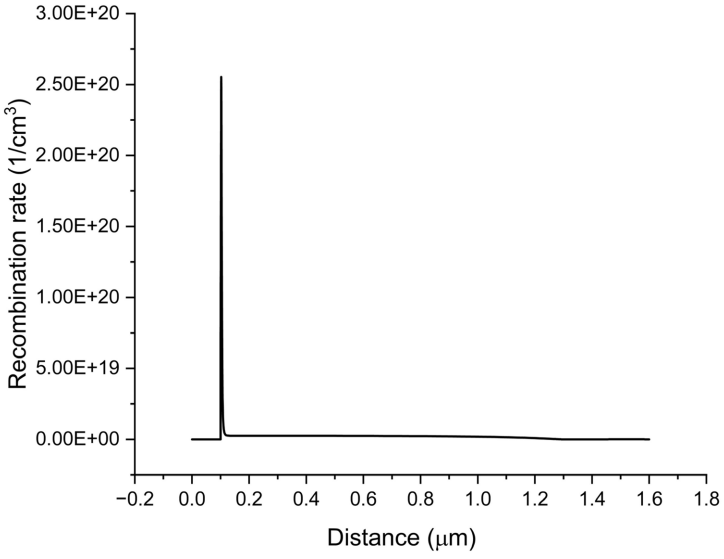

Figure 16. Recombination rate distribution in K_2TiI_6-Based devices.

Overall, it performs better at intermediate bias voltages, whereas it shows enhanced performance at higher bias, with improved generation and relatively steady recombination. These trends imply that each material can be fine-tuned for optimal performance in specific voltage operating ranges, thereby supporting the design of bias-optimized PV devices.

4. Conclusion

This work proposes a novel FTO/CdZnS/K_2TiI_6/D-PBTTT-14/Au structure for a highly efficient, lead-free, and sustainable perovskite solar cell (PSC) based on K_2TiI_6. The effects of different ETL materials on device performance are investigated, along with improvements in several solar cell characteristics and operational parameters. Furthermore, the performance is evaluated based on already published literary works. The FF of the suggested structure is 86.5%, a 24.42 mA/cm^2 Jsc, an efficiency of 28%, and a 1.33 V Voc. We also looked at the impacts of operating temperature, series and shunt resistance, and the thickness of the K_2TiI_6 and ETL. Additionally, the consequences of C-V properties such as Mott-Schottky and capacitance, as well as Quantum efficiency, J-V properties, and generation and recombination rates, were also evaluated. Additionally, the structure displays superior quantum efficiency in the visible and near-infrared spectrums. Ideally, going forward, this research will contribute to the creation of SCs devoid of lead, which can provide a basis for more adaptable and stable technology. The maximum PCE of 28.11% with Voc of 1.33 V, Jsc of 24.42 mA/cm^2, and FF of 86.50% was demonstrated by the ETL and HTL-based heterojunction with FTO/CdZnS/K_2TiI_6/D-PBTTT-14/Au device configuration out of the three optimized devices.

Funding

The research works have been conducted by self-funded.

Data Availability

The study's data can be obtained from the corresponding author upon a reasonable request.

Acknowledgements

We express our gratitude to the Department of Electrical and Electronic Engineering at Hajee Mohammad Danesh Science and Technology University, Dinajpur-5200, Bangladesh, for their essential technical assistance.

Conflicts of Interest

The authors assert that there are no conflicts of interest about the publishing of this work.

References

[1] Hasan, M.M., Hossain, S., Mofijur, M., Kabir, Z., Badruddin, I.A., Yunus Khan, T.M.,

et al. (2023) Harnessing Solar Power: A Review of Photovoltaic Innovations, Solar Thermal Systems, and the Dawn of Energy Storage Solutions. *Energies*, **16**, Article 6456. https://doi.org/10.3390/en16186456

[2] Song, Z., McElvany, C.L., Phillips, A.B., Celik, I., Krantz, P.W., Watthage, S.C., *et al.* (2017) A Technoeconomic Analysis of Perovskite Solar Module Manufacturing with Low-Cost Materials and Techniques. *Energy & Environmental Science*, **10**, 1297-1305. https://doi.org/10.1039/c7ee00757d

[3] Park, N.G. (2015) Perovskite Solar Cells: An Emerging Photovoltaic Technology. *Materials Today*, **18**, 65-72. https://doi.org/10.1016/j.mattod.2014.07.007

[4] Green, M.A., Ho-Baillie, A. and Snaith, H.J. (2014) The Emergence of Perovskite Solar Cells. *Nature Photonics*, **8**, 506-514. https://doi.org/10.1038/nphoton.2014.134

[5] Saliba, M., Matsui, T., Domanski, K., Seo, J., Ummadisingu, A., Zakeeruddin, S.M., *et al.* (2016) Incorporation of Rubidium Cations into Perovskite Solar Cells Improves Photovoltaic Performance. *Science*, **354**, 206-209. https://doi.org/10.1126/science.aah5557

[6] Leijtens, T., Eperon, G.E., Noel, N.K., Habisreutinger, S.N., Petrozza, A. and Snaith, H.J. (2015) Stability of Metal Halide Perovskite Solar Cells. *Advanced Energy Materials*, **5**, Article 1500963. https://doi.org/10.1002/aenm.201500963

[7] Walsh, A. (2015) Principles of Chemical Bonding and Band Gap Engineering in Hybrid Organic-Inorganic Halide Perovskites. *The Journal of Physical Chemistry C*, **119**, 5755-5760. https://doi.org/10.1021/jp512420b

[8] Patel, A.M., Kumavat, S.R. and Sonvane, Y. (2025) Exploring Inorganic Mixed-Halide Perovskites CsSn(I1-nBrn)3 and $CsSn(Br_{1-n}Cln)_3$ for High Power Efficiency. *Materials Chemistry and Physics*, **341**, Article 130913. https://doi.org/10.1016/j.matchemphys.2025.130913

[9] Kumar, S. and Murugesan, M. (2022) Lead-Free and Stable Potassium Titanium Halide Perovskites: Synthesis, Characterization and Solar Cell Simulation. *Energies*, **15**, Article 6963. https://doi.org/10.3390/en15196963

[10] Singh, N., Agarwal, A. and Agarwal, M. (2024) Numerical Investigation of the Pb-Free Titanium-Based Double-Perovskite Solar Cell. *Journal of Nanoparticle Research*, **26**, Article No. 137. https://doi.org/10.1007/s11051-024-06038-8

[11] Zein, W., Alanazi, T.I., Salah, M.M. and Saeed, A. (2023) Concurrent Design of Alloy Compositions of CZTSSe and CdZnS Using SCAPS Simulation: Potential Routes to Overcoming VOC Deficit. *Energies*, **16**, Article 5754. https://doi.org/10.3390/en16155754

[12] Wei, Z., Zhou, Q., Niu, X., Liu, S., Dong, Z., Liang, H., *et al.* (2025) Surpassing 90% Shockley-Queisser VOC Limit in 1.79 eV Wide-Bandgap Perovskite Solar Cells Using Bromine-Substituted Self-Assembled Monolayers. *Energy & Environmental Science*, **18**, 1847-1855. https://doi.org/10.1039/d4ee04029e

[13] Wang, K., Zheng, L., Hou, Y., Nozariasbmarz, A., Poudel, B., Yoon, J., *et al.* (2022) Overcoming Shockley-Queisser Limit Using Halide Perovskite Platform? *Joule*, **6**, 756-771. https://doi.org/10.1016/j.joule.2022.01.009

[14] Green, M.A., Hishikawa, Y., Dunlop, E.D., Levi, D.H., Hohl-Ebinger, J., Yoshita, M., *et al.* (2019) Solar Cell Efficiency Tables (Version 53). *Progress in Photovoltaics: Research and Applications*, **27**, 3-12. https://doi.org/10.1002/pip.3102

[15] Banik, S., Das, A., Das, B.K. and Islam, N. (2024) Numerical Simulation and Performance Optimization of a Lead-Free Inorganic Perovskite Solar Cell Using SCAPS-1D. *Heliyon*, **10**, e23985. https://doi.org/10.1016/j.heliyon.2024.e23985

[16] Hossain, M.K., Sadat, K.M., Uddin, M.S., Datta, A.K., Kanjariya, P., Reddy, M.S., *et al.* (2025) An Investigation of Hole Transport Layers and Electron Transport Layers to Produce Highly Efficient K2TII6-Based Perovskite Solar Cells. *Scientific Reports*, **15**, Article No. 19014. https://doi.org/10.1038/s41598-025-98351-y